Kovove Mater. 59 2021 237–244
DOI: 10.4149/km_2021_4_237

Graphene nanoplatelets reinforced aluminum alloy matrix composites produced by spark plasma sintering

V. Puchý[1]*, M. Podobová[1], R. Džunda[1], P. Hvizdoš[1], O. Velgosová[2], M. Besterci[1], B. Ballóková[1]

[1]*Institute of Materials Research, SAS, Watsonova 47, 040 01 Košice, Slovak Republic*
[2]*Faculty of Materials, Metallurgy and Recycling TUKE, Letná 9, 042 00 Košice, Slovak Republic*

Received 31 May 2021, received in revised form 6 July 2021, accepted 8 August 2021

Abstract

Aluminum alloys (A.A.) are interesting for their low weight and good mechanical properties. The addition of graphene nanoplatelets (GNPs) can reduce the density and modify the functional properties and mechanical performance of the metal matrix. Graphene reinforced A.A. matrix composites (AA-GNPs) were prepared by spark plasma sintering technique (SPS), using commercial graphene nanoplatelets mixed with recycled milled A.A. chips. Monolithic A.A. and aluminum composites with 2.5 wt.% of GNPs (AA-2.5GNPs) were compacted into disc-shaped samples. The microstructure was studied and characterized by optical (O.M.) and scanning electron (SEM) microscopies. Hardness was measured, and tribological properties were studied by the ball-on-disc technique. The coefficients of friction and wear rates were evaluated. Worn surfaces were studied by SEM and confocal microscopy, and the oxidation level was measured using EDX spectrometry. The developed process presented here provides promising results for preparing AA-2.5GNPs nanocomposites from low-cost recycled A.A. chips with SPS.

K e y w o r d s: aluminum alloy, aluminum matrix composites, graphene nanoplatelets, spark plasma sintering, wear

1. Introduction

Properties of aluminum-matrix alloys, low weight, and very good mechanical behavior are the reason why they are so interesting. The field of wide applications of this high-conductivity metal, including Mg, Cu and others, and aluminum matrix composites, is not only in electronics and electrical engineering [1] but have also been designed for high-tech and functional applications including aerospace, defense, automotive, thermal management, sports and recreation, electronic packaging, and armor [2]. With an ambition to shape up both mechanical and tribological properties, and as well electrical conductivity, these metal matrix composites are strengthened by the addition of different ceramic materials such as ZrO_2 [3], Al_2O_3, SiC [4, 5], B_4C [6, 7], etc.; metal powders like W are possible to be used for anti-radiation protection [7]. For reduction of the density and metal matrix properties modification, a suitable choice is the use of graphene. Graphene, defined by superior tensile strength values 130 GPa and Young's modulus 1 TPa, is a hopeful nominee to act as a reinforcing material in metal matrix nanocomposites [8, 9]. Due to its electrical conductivity, there is a prospect of using these materials in power transmission lines [10]. The history of the study of aluminum matrix composites (AMCs) dates to 1920; since then, much attention has been paid to this research. Carbon as a reinforcing allowance can be used in different forms, as carbon nanotubes or as graphene nanoparticles [11–13], graphene nano-flakes (GNF) [12–15], multilayer graphene (FLG) [16] or its derivatives: graphene oxide and reduced graphene oxide [17, 18]. Single layers of graphene were first produced in 2004 by Novoselov et al. [19, 20]. Until then, popular solutions have been to use conventional AMCs reinforcements, such as equiaxial ceramics, short fibers, whiskers, continuous fibers, and

*Corresponding author: e-mail address: vpuchy@saske.sk

monofilament [2]. Few-layer graphene (FLG) is defined by 3 to 9 layers, and the layer number limit when graphene becomes graphite is 10 layers. The atomic structure of graphene results in exceptional electrical, optical, mechanical, and thermal properties [21]. Besides graphene, carbon nanotubes have excellent mechanical and physical properties, such as ultra-high strength and electrical conductivity, and are therefore expected to be used as reinforcing additives to improve the mechanical and electrical properties of conductive metallic materials [22]. Nonetheless, previous research has shown that the strength of pure metals can be increased by using carbon nanotubes (CNTs) as reinforcement, but the electrical conductivity of these nanocomposites was always lower compared to pure metals [23–30]. Ebbesen et al. [31] and Wang et al. [32] measured CNT and graphene electrical conductivity. The results showed that the electrical conductivity of graphene ($\sim 67\,\mathrm{MS\,m^{-1}}$) was significantly higher than that of CNT ($\sim 20\,\mathrm{MS\,m^{-1}}$). Therefore, attention is focused on graphene as a reinforcing parameter [33]. The requirement for producing these metal matrix reinforced composites is to obtain strong, solid, and cost-effective materials for existing and future technologies [34]. More emphasis is placed on the production as environmentally friendly as possible (e.g., using waste from processing pure metals or its alloys).

This study aimed to develop and present the fabrication process of AA-2.5GNP composites by SPS technique using low-cost recycled A.A. chips.

2. Materials and methods

A.A. chips (Fig. 1a) used in this work were produced from a CNC machining centrum with varying processing speeds and amounts of lubrication. This resulted in thickness variation ranging from approximately 0.5 to 2 mm and a variable length with some chips exceeding 100 mm. The chip morphology can be related to the tool wear and the surface integrity of the machined part. The microstructure change on the machined surface of the chip typically manifests as the layer with homogenous or ultrafine grain microstructure. The layer is generated mainly from the phase transformation from rapid heating and quenching and from severe plastic deformation. All A.A. chips were degreased with acetone and dried in an oven. Before further processing, grinding was executed to get a more homogenous and finer blend of chips-powder, averaging in diameter under 100 µm to eliminate possible size effects regarding sintering and further mixing with graphene. All prepared samples were based on EN AW 5083 aluminum alloy marked as A.A.; their structures may differ depending on the amount of temperature arising from machining. These variations can be seen by varying amounts of the darker intermetallic magnesium silicide (Mg_2Si) phase. The brighter and more evenly distributed intermetallic phase mainly consists of iron, manganese, and silicon alloying elements and builds an undissolved and more evenly distributed always present phase of Al(FeMn)Si as published in [35]. Additional deformation at elevated temperature promotes oxide breakage caused by a wider

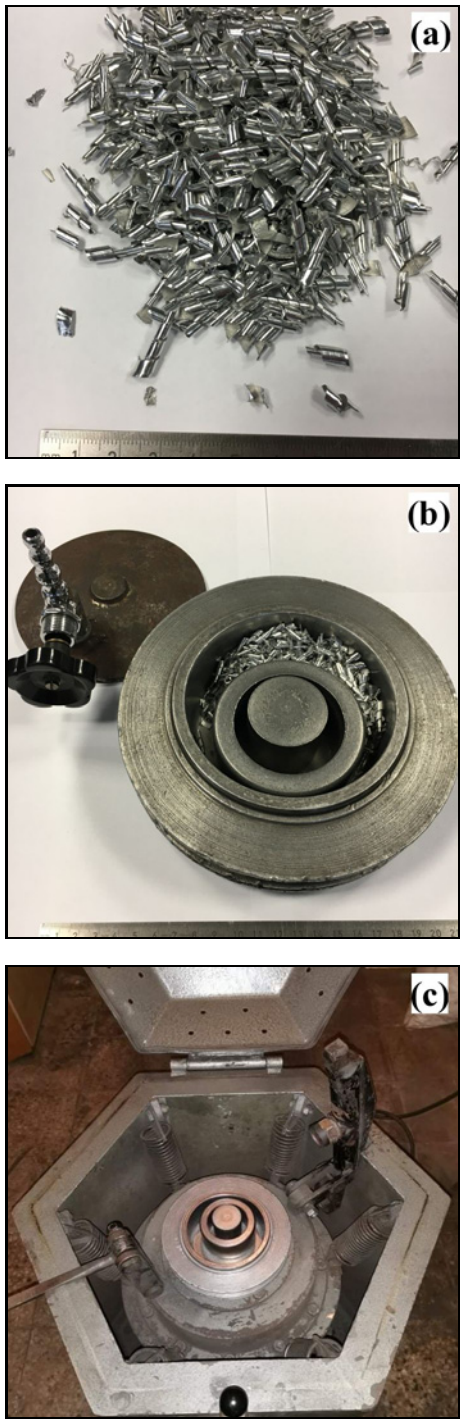

Fig. 1. Morphology of monolithic A.A. chips (a), milling disk chamber (b), and vibrational mill (c).

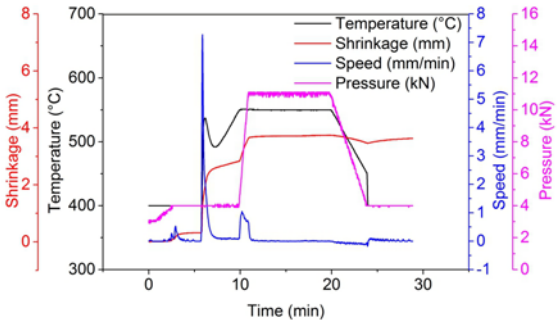

Fig. 2. Preset temperature, pressure, piston speed, and shrinkage curves used during fabrication of spark plasma sintering (SPS) specimens with a maximum load of 11 kN, equaling an applied pressure of 50 MPa.

spread between the hardness values of base metal and the brittle surface oxide [36, 37]. The size reduction of aluminum alloy chips was conducted in a vibrational "UFO" disc mill (home-made at IMR SAS, Slovakia). The mill (Figs. 1b,c) consists of a 300 ml working chamber with a high-alloyed stainless-steel ring (ø 70 mm).

The milling period was set at 20 min. The exit sieve with 55 µm mesh size holes was used. After that, the 20 g A.A. powder was added together with 0.5 g GNPs and 10 stainless steel balls into the 3D Turbula mixer and mechanically mixed for 30 min. The SPS with a graphite tool assembly was used to produce specimens with a processing temperature of 550 ℃ and a maximum sintering pressure of 50 MPa. As shown in Fig. 2, specimens were heated to 550 ℃ within 10 minutes, followed by 10 minutes of holding at peak temperature and a controlled cooling step within seven minutes. For comparison, a pure A.A. sample was also fabricated under the same condition. The final samples had a disc shape with 3 mm thickness and 20 mm diameter. Sintered samples were polished using series of diamond suspensions from 30 to 1 µm. The average grain size of each composite was determined using the line method on scanning electron microscopy (SEM) images, and the density was determined by Archimedes' method. Tribology tests were performed on an automatic tribometer (Bruker, USA) in reciprocating dry sliding conditions, using a ball-on-disc geometry at room temperature and pressure. A 100Cr6 steel ball with a 6 mm diameter was used as a tribo partner. All tests were carried out under 2 N normal load, 0.1 m s^{-1} sliding velocity, and 5 mm stroke length. The total sliding distance was 50 m. The coefficient of friction (COF) was calculated by taking the ratio of the tangential and normal forces, and it was reported versus the sliding distance. The volume removed was measured using confocal microscopy, where a hundred layers along the depth of the track were recorded. The wear rate, W, was determined in terms of the volume loss V per distance L and applied load F according to the following Eq. (1):

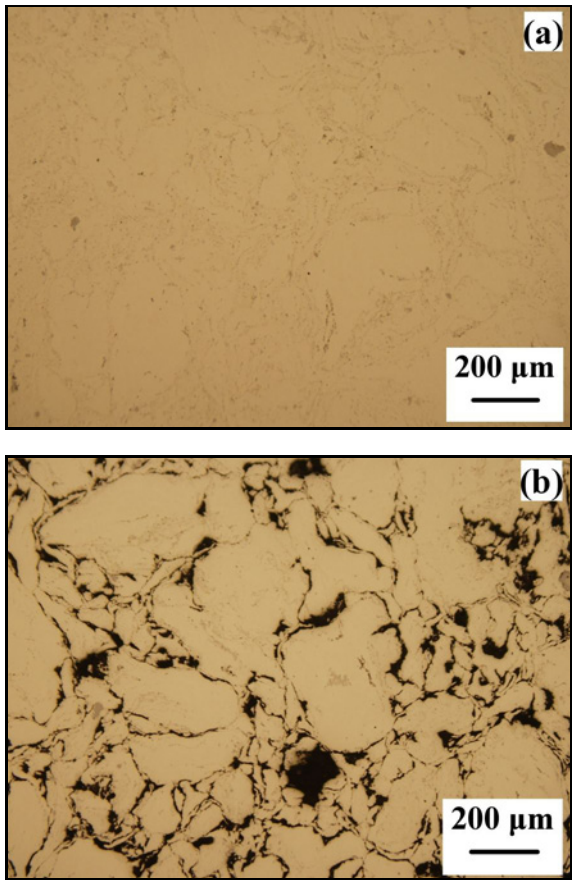

Fig. 3. O.M. images showing sample microstructure: monolithic A.A. (a) and AA-2.5GNPs composite (b).

$$W = \frac{V}{L \times F}. \tag{1}$$

3. Results and discussion

3.1. Microstructure and hardness

The microstructures of monolithic A.A. and AA-2.5GNPs composite produced by SPS method were examined by Olympus O.M. (Figs. 3a,b). Optical microstructural analysis showed that in the monolithic A.A. material, a dense microstructure with very low porosity was found. In the AA-2.5GNPs composite material, the distribution of GNPs was determined. According to analyses, it was observed that GNPs are distributed around individual grains and create an electrically conductive grid that can enhance the sintering process. The hardness of sintered monolithic A.A. and AA-2.5GNPs composite samples measured using Vickers indentation technique with a load of 25 g

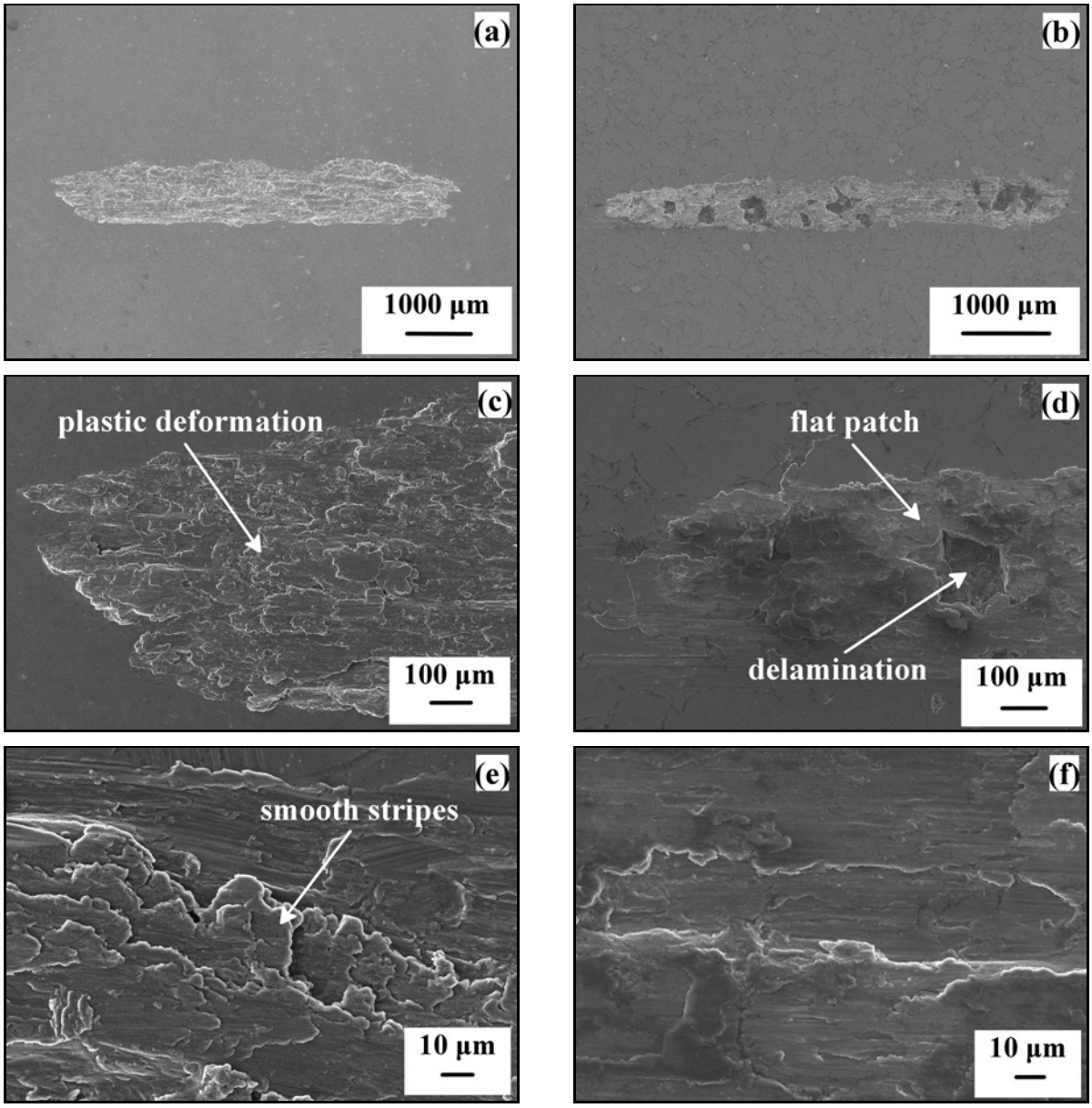

Fig. 4. SEM micrographs of wear tracks on A.A. (a, c, e) and AA-2.5GNPs composite (b, d, f) at translation speed of $0.1\,\mathrm{m\,s^{-1}}$, length of 50 m and friction force of 2 N, obtained from wear tests under dry conditions.

was approximately $100\,\mathrm{HV}_{0.025}$ and $109\,\mathrm{HV}_{0.025}$, respectively. According to literature, hardness values of the A.A. alloys depending on heat treatment temperature and aging time are in the range of 75 HV [38]. The relative density of the samples calculated according to Archimedes' principle was approximately 99.5 and 97.5 %, respectively.

3.2. Tribological properties, coefficient of friction, and wear

Figure 4 shows the microstructure of wear tracks generated on the worn surfaces of A.A. and AA-2.5GNPs composite resulted from the tests under dry conditions at R.T. in reciprocating sliding after 50 m sliding distance. Figures 4c,e – the corresponding magnified images of Fig. 4a – reveal the morphology of the A.A. friction zone from wear track and Figs. 4d,f the corresponding magnified images of Fig. 4b of the AA-2.5GNPs composite, respectively. It was observed that the plastic deformation of the wear tracks becomes less severe at AA-2.5GNPs composite. The severe plastic deformation with smeared surfaces occured due to the stronger adhesion between the friction ball and the samples during the tests. The addition of graphene to the A.A. matrix caused release/pulling out of GNPs particles at the friction, which had a positive effect on decreasing the coefficient of friction. This could be related to a decrease in abrasion by forming some friction film during sliding,

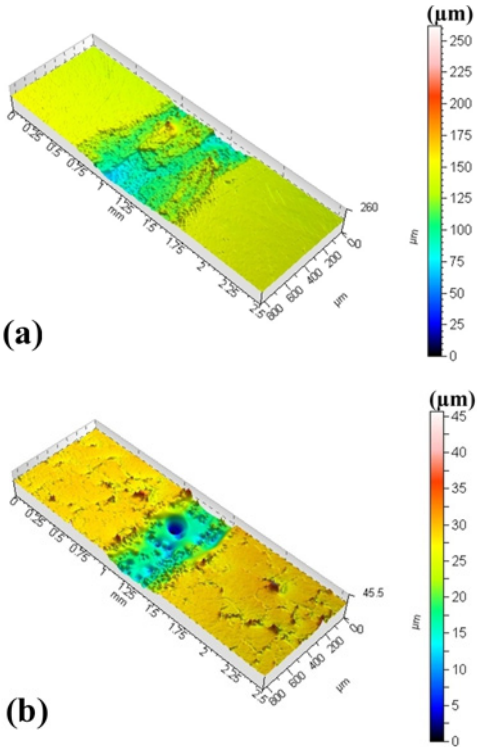

Fig. 5. Axonometric plots of wear tracks on A.A. (a) and AA-2.5GNPs composite (b) at translation speed of 0.1 m s^{-1}, length of 50 m, and friction force of 2 N, obtained from wear tests under dry conditions.

related to the flat patches observed on the wear track. In Fig. 5a, many flat patches were observed, and an apparent increase in the depth and increase in the width of the track profile of monolithic A.A. as in Fig. 5b, the corresponding axonometric plot of AA-2.5GNPs composite. Therefore, more severe surface traction is exerted towards the direction of the sample translation by normal and tangential loads at the monolithic A.A. sample. The appearance of smooth stripes illustrates the plastic deformation of the sample surface created in the sliding (Fig. 4e). These typical properties represent the typical abrasive wear behavior [39]. Compared with the A.A. sample, the number of debris in the AA-2.5GNPs samples is markedly decreased, and the delamination is reduced. It is clear from Fig. 4 that GNPs disperse uniformly on the wear surface with little debris and furrows, which infers that the presence of GNPs is beneficial to reduce the wear rate due to the low shear force and friction coefficient between graphene layers.

The typical mechanisms for AA-2.5GNPs composite can be summarized as follows: The GNPs form a carbon friction film, which covers the surface and acts as a solid lubricant, reducing the COF of composite. The high thermal conductivity of GNPs improves the thermal conductivity of the matrix [40], which reduces the heat and keeps the hardness and strength of the

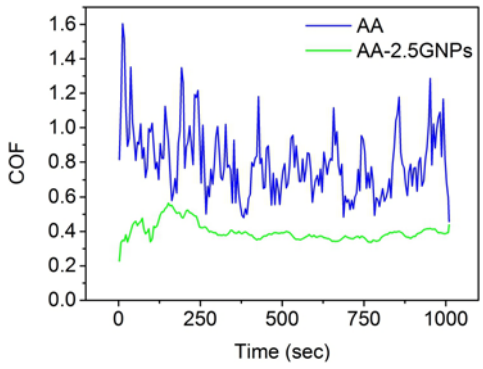

Fig. 6. COF vs. time graphs of A.A. and AA-2.5GNPs composite at translation speed of 0.1 m s^{-1}, length of 50 m and friction force of 2 N, obtained from wear tests under dry conditions.

composite in the wear test. The contact area between the ball and the disc decreases, thus contributing to the reduction and stability of the COF.

The GNPs embedded in the A.A. matrix were found to significantly enhance not only the microhardness and COF but also the wear resistance of the composites due to its tribological effect. By adding a GNPs phase, the depth and width of the wear track decrease, as is documented in Figs. 5a,b. The COF decreased from 0.8 for A.A. to 0.4 for AA-2.5GNPs (Fig. 6). Figure 6 shows the friction coefficient curves of the specimens. At the beginning of the dry sliding wear test, the initial friction coefficient varies between 0.2 and 0.8 for the AA-2.5GNPs composite and the monolithic A.A. specimens. After approximately 1 m of sliding distance, the friction coefficients raised about 0.4 and 0.85 for the AA-2.5GNPs composite and the monolithic A.A. specimens, respectively. The friction coefficients curves are unequal with both abrasion and adhesion phenomena. The average friction coefficient decreased with the addition of GNPs particles and the increasing hardness of the AA-2.5GNPs composite specimen. It is known that some materials, e.g., steels [41] with harder phases, provide a lower friction coefficient. However, heterogeneity of coarse GNPs dispersion and higher hardness of composite slightly decreased the relative density and raised the delamination effect (Fig. 4). EDS analysis in Fig. 7a shows that the main composition of the A.A. debris region is Mg and Al. The beneficial effect of adding GNPs in the A.A. matrix and potential to create friction film, a C is displayed by EDS in Fig. 7b. In the regime of friction cycle under 2 N normal load, 0.1 m s^{-1} sliding speed, 50 m wear cycle, the use of GNPs as an additive (2.5 wt.%) in the A.A. matrix resulted in a marked reduction of the wear rate from 144.1 to 35.6 $\times$ 10^{-5} mm^3 N^{-1} m^{-1}.

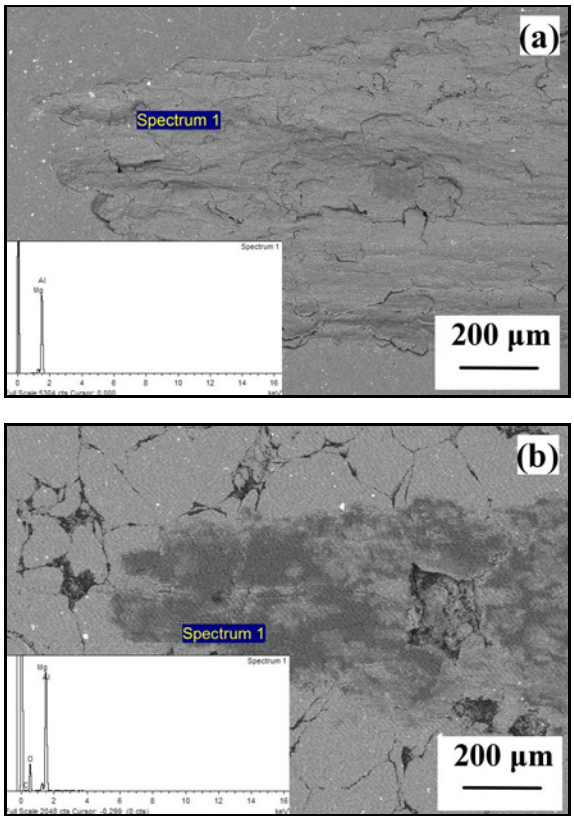

Fig. 7. SEM micrographs with EDS analyses of wear tracks on A.A. (a) and AA-2.5GNPs composite (b) at translation speed of 0.1 m s^{-1}, length of 50 m and friction force of 2 N, obtained from wear tests under dry conditions.

4. Conclusions

Monolithic A.A. and AA-2.5GNPs composite materials using low-cost A.A. chips (leftovers from machining) were successfully prepared by SPS in a vacuum. The fabricated materials have a dense microstructure and low porosity. The addition of GNPs resulted in enhanced hardness, which was 100 HV for the reference materials and 109 HV for the composite. The wear characteristics of the two materials were evaluated under dry conditions at room temperature.

Among the key findings are the following: The wear rate of the A.A. material is approximately four times higher than that of the Al-2.5GNPs composite. The main reason is the graphene friction film formed between the friction pair, which acts as a solid lubricant. This leads to the reduction of friction forces and adhesion. The coefficient of friction decreased from ∼ 0.8 for the A.A. down to ∼ 0.4 for the AA-GNP composite. The plastic deformation of the wear tracks was more severe in monolithic material and resulted from the stronger adhesion between the ball and the surface of samples formed under dry conditions. Yet, in both materials, the principal wear micromechanism appeared to be adhesion accompanied by ploughing and occasional delamination.

Overall, the work confirmed a positive influence of SPS on the compaction of A.A. chips with GNPs as an additive, but further work will be necessary to achieve homogenous bonding and decrease the delamination effect required for an industrial application. Further optimization of sintering process parameters may deliver more suitable processing, leading to superior performance. A combination of grinding with mixing in a high-energy ball mill (Attritor, for example) may be used to enhance bonding additionally. The AA-2.5GNPs composites could extend the lifetime of recycled aluminum materials, offering higher mechanical properties to weight ratios for typical AMCs applications. However, even with the observed reinforcing effects, there still exist challenges for using these nanomaterials as reinforcement in A.A. composites which require further research.

Acknowledgements

This work was supported by the projects APVV-18--0438 and VEGA 2/0101/20.

References

[1] L. Lu, Y. Shen, X. Chen, L. Qian, K. Lu, Ultrahigh strength and high electrical conductivity in copper, Science 304 (2004) 422–426. doi:10.1126/science.1092905

[2] M. K. Surappa, Aluminium matrix composites: challenges and opportunities, Sadhana 28 (2003) 319–334. doi:10.1007/BF02717141

[3] S. B. Boppana, S. Dayanand, A. Kumar MR, V. Kumard, A. Ta, Synthesis and characterization of nano graphene and ZrO_2 reinforced Al 6061 metal matrix composites, J. Mater. Res. Technol. 9 (2020) 7354–7362. doi:10.1016/j.jmrt.2020.05.013

[4] S. Veličković, S. Garić, B. Stojanović, A. Vencl, Tribological properties of aluminium matrix nanocomposites, App. Eng. Lett. 1 (2016) 72–79.

[5] M. O. Bodunrin, K. K. Alanemea, L. H. Chown, Aluminium matrix hybrid composites: A review of reinforcement philosophies; mechanical, corrosion and tribological characteristics, J. Mater. Res. Technol. 4 (2015) 434–445. doi:10.1016/j.jmrt.2015.05.003

[6] E. Ghasali, M. Alizadeh, M. Niazmand, T. Ebadzadeh, Fabrication of magnesium-boron carbide metal matrix composite by powder metallurgy route: Comparison between microwave and spark plasma sintering, J. Alloy Compd. 697 (2017) 200–207. doi:10.1016/j.jallcom.2016.12.146

[7] E. S. Dvilis, O. L. Khasanov, V. N. Gulbin, M. S. Petyukevich, A. O. Khasanov, E. A. Olevsky, Spark plasma sintering of aluminum-magnesium-matrix composites with boron carbide and tungsten nano-powder inclusions: Modeling and experimentation, JOM-J.

Min. Met. Mat. S 68 (2016) 908–919. doi:10.1007/s11837-015-1781-1
[8] I. A. Ovidko, Mechanical properties of graphene, Rev. Adv. Mater. Sci. 34 (2013) 1–11.
[9] C. Lee, X. Wei, J. W. Kysar, J. Hone, Measurement of the elastic properties and intrinsic strength of monolayer graphene, Science 321 (2008) 385–388. doi:10.1126/science.1157996
[10] J. Liu, U. Khan, J. Coleman, B. Fernandez, P. Rodriguez, S. Naher, D. Brabazon, Graphene oxide and graphene nanosheet reinforced aluminium matrix composites: Powder synthesis and prepared composite characteristics, Mater. Design 94 (2016) 87–94. doi:10.1016/j.matdes.2016.01.031
[11] S. F. Bartolucci, J. Paras, M. A. Rafiee, J. Rafiee, S. Lee, D. Kapoor, N. Koratkar, Graphene–aluminum nanocomposites, Mat. Sci. Eng. A-Struct. 528 (2011) 7933–7937. doi:10.1016/j.msea.2011.07.043
[12] S.-J. Yan, Y. Cheng, H. Qi-Hu, C. Jun-Zou, L. Da--Bo, D. Sheng-Long, Research of graphene-reinforced aluminum matrix nanocomposites, J. Mater. Eng. 4 (2014) 1–6. doi:10.3969/j.issn.1001-4381.2014.04.001
[13] A. F. Boostani, S. Tahamtan, Z. Jiang, D. Wei, S. Yazdani, R. A. Khosroshahi, R. T. Mousavian, J. Xu, X. Zhang, D. Gong, Enhanced tensile properties of aluminium matrix composites reinforced with graphene encapsulated SiC nanoparticles, Compos. Part A – Appl. S 68 (2015) 155–163. doi:10.1016/j.compositesa.2014.10.010
[14] J. L. Li, Y. C. Xiong, X. D. Wang, S. J. Yan, C. Yang, W. W. He, J. Z. Chen, S. Q. Wang, X. Y. Zhang, S. L. Dai, Microstructure and tensile properties of bulk nanostructured aluminum/graphene composites prepared via cryomilling, Mat. Sci. Eng. A-Struct. 626 (2015) 400–405. doi:10.1016/j.msea.2014.12.102
[15] M. Rashad, F. Pan, A. Tang, M. Asif, Effect of graphene nanoplatelets addition on mechanical properties of pure aluminum using a semi-powder method, Prog. Nat. Sci.: Mater. Int. 24 (2014) 101–108. doi:10.1016/j.pnsc.2014.03.012
[16] S. E. Shin, H. J. Choi, J. H. Shin, D. H. Bae, Strengthening behavior of few-layered graphene/aluminum composites, Carbon 82 (2015) 143–151. doi:10.1016/j.carbon.2014.10.044
[17] Z. Li, G. Fan, Z. Tan, Q. Guo, D. Xiong, Y. Su, Z. Li, D. Zhang, Uniform dispersion of graphene oxide in aluminum powder by direct electrostatic adsorption for fabrication of graphene/aluminum composites, Nanotechnology 25 (2014) 325601. doi:10.1088/0957-4484/25/32/325601
[18] J. Wang, Z. Li, G. Fan, H. Pan, Z. Chen, D. Zhang, Reinforcement with graphene nanosheets in aluminum matrix composites, Scripta Mater. 66 (2012) 594–597. doi:10.1016/j.scriptamat.2012.01.012
[19] K. S. Novoselov, A. K. Geim, S. V. Morozov, D. Jiang, Y. Zhang, S. V. Dubonos, I. V. Grigorieva, A. A. Firsov, Electric field effect in atomically thin carbon films, Science 306 (2004) 666–669. doi:10.1126/science.1102896
[20] F. A. Chyada, A. R. Jabur, H. A. Alwan, Effect addition of graphene on electrical conductivity and tensile strength for recycled electric power transmission wires, Energy Proceed. 119 (2017) 121–130. doi:10.1016/j.egypro.2017.07.055
[21] A. K. Geim, K. S. Novoselov, The rise of graphene, Nat. Mater. 6 (2007) 183–191. doi:10.1038/nmat1849
[22] O. Hjortstam, P. Isberg, S. Soderholm, H. Dai, Can we achieve ultra-low resistivity in carbon nanotube-based metal composites?, Appl. Phys. A-Mater. 78 (2004) 1175–1179. doi:10.1007/s00339-003-2424-x
[23] Y. Feng, H. L. Yuan, M. Zhang, Fabrication and properties of silver-matrix composites reinforced by carbon nanotubes, Mater. Charact. 55 (2005) 211–218. doi:10.1016/j.matchar.2005.05.003
[24] C. Subramaniam, T. Yamada, K. Kobashi, A. Sekiguchi, D. N. Futaba, M. Yumura, K. Hata, One hundred fold increase in current carrying capacity in a carbon nanotube-copper composite, Nat. Commun. 4 (2013) 2202. doi:10.1038/ncomms3202
[25] S. M. Uddin, T. Mahmud, C. Wolf, C. Glanz, I. Kolaric, C. Volkmer, H. Höller, U. Wienecke, S. Roth, H.-J. Fecht, Effect of size and shape of metal particles to improve hardness and electrical properties of carbon nanotube reinforced copper and copper alloy composites, Compos. Sci. Technol. 70 (2010) 2253–2257. doi:10.1016/j.compscitech.2010.07.012
[26] W. M. Daoush, B. K. Lim, C. B. Mo, D. H. Nam, S. H. Hong, Electrical and mechanical properties of carbon nanotube reinforced copper nanocomposites fabricated by electroless deposition process, Mat. Sci. Eng. A-Struct. 513–514 (2009) 247–253. doi:10.1016/j.msea.2009.01.073
[27] C. L. Xu, B. Q. Wei, R. Z. Ma, J. Liang, X. K. Ma, D. H. Wu, Fabrication of aluminum-carbon nanotube composites and their electrical properties, Carbon 37 (1999) 855–858. doi:10.1016/S0008-6223(98)00285-1
[28] Z. Y. Liu, B. L. Xiao, W. G. Wang, Z. Y. Ma, Tensile strength and electrical conductivity of carbon nanotube reinforced aluminum matrix composites fabricated by powder metallurgy combined with friction stir processing, J. Mater. Sci. Technol. 30 (2014) 649–655. doi:10.1016/j.jmst.2014.04.016
[29] B. Chen, S. Li, H. Imai, L. Jia, J. Umeda, M. Takahashi, K. Kondoh, Carbon nanotube induced microstructural characteristics in powder metallurgy Al matrix composites and their effects on mechanical and conductive properties, J. Alloy. Compd. 651 (2015) 608–615. doi:10.1016/j.jallcom.2015.08.178
[30] W. Zhou, G. Yamamoto, Y. Fan, H. Kwon, T. Hashida, A. Kawasaki, In-situ characterization of interfacial shear strength in multi-walled carbon nanotube reinforced aluminum matrix composites, Carbon 106 (2016) 37–47. doi:10.1016/j.carbon.2016.05.015
[31] T.W. Ebbesen, H. J. Lezec, H. Hiura, J. W. Bennett, H. F. Ghaemi, T. Thio, Electrical conductivity of individual carbon nanotubes, Nature 382 (1996) 54–56. doi:10.1038/382054a0
[32] L. Wang, I. Meric, P. Y. Huang, Q. Gao, Y. Gao, H. Tran, T. Taniguchi, K. Watanabe, L. M. Campos, D. A. Muller, J. Guo, P. Kim, J. Hone, K. L. Shepard, C. R. Dean, One-dimensional electrical contact to a two-dimensional material, Science 342 (2013) 614–617. doi:10.1126/science.1244358
[33] S. Zhang, G. Chen, T. Qu, G. Fang, S. Bai, Y. Yan, G. Zhang, Z. Zhou, J. Shen, D. Yao, Y. Zhang, Q. Shi, Simultaneously enhancing mechanical properties and

electrical conductivity of aluminum by using graphene as the reinforcement, Mater. Lett. 265 (2020) 127440. doi:10.1016/j.matlet.2020.127440

[34] I. A. Oviďko, Metal-graphene nanocomposites with enhanced mechanical properties: A review, Rev. Adv. Mater. Sci. 38 (2014) 190–200.

[35] B. Milkereit, Kontinuierliche Zeit-Temperatur-Ausscheidungs-Diagramme von Al-Mg-Si-Legierungen. Ph.D. Thesis, University of Rostock, Rostock, 2010. https://www.shaker.de/de/content/catalogue/index.asp?lang=de&ID=8&ISBN=978-3-8322-9993-4

[36] C. N. Cislo, T. Fazokas, B. Buchmayr, Ch. Weiß, Consolidation behaviour of aluminium alloy machining chips during the high pressure torsion process. In the Conference Proceedings of XXXVIII. Verformungskundlichen Kolloquium, Zauchensee, 2019, pp. 114–119.

[37] C. N. Cislo, B. Kronthaler, B. Buchmayr, Ch. Weiß, Solid state recycling of aluminum alloy chips via pulsed electric current sintering, J. Manuf. Mater. Process. 4 (2020) 23. doi:10.3390/jmmp4010023

[38] https://www.thyssenkrupp-materials.co.uk/aluminium-5083.html

[39] Y.-S. Lee, Y. Kondo, M. Okayasu, Friction-induced martensitic transformation and wear properties of stainless steel under dry and wet conditions, Metals 10 (2020) 743. doi:10.3390/met10060743

[40] G. Xie, O. Ohashi, M. Song, K. Furuya, T. Noda, Behavior of oxide film at the interface between particles in sintered Al powders by pulse electric-current sintering, Metall. Mater. Trans. A 34 (2003) 699–703. doi:10.1007/s11661-003-0104-2

[41] A. Güral, Influence of martensite particle size on dry sliding wear behaviour of low carbon dual phase powder metallurgy steels, Kovove Mater. 48 (2010) 25–31. doi:10.4149/km_2010_1_25